

The Suppression of CMR in $\text{NdMn}_{1-x}\text{Co}_x\text{AsO}_{0.95}\text{F}_{0.05}$

E. J. Wildman¹, K. S. McCombie¹, G. B. G. Stenning² and A. C. Mclaughlin^{1*}

¹ The Chemistry Department, University of Aberdeen, Meston Walk, Aberdeen, AB24 3UE, Scotland.

² ISIS, Science and Technology Facilities Council, Rutherford Appleton Laboratory, Didcot, OX11 0QX, UK.

Abstract

The colossal magnetoresistance (CMR) observed in the oxypnictide $\text{NdMnAsO}_{1-x}\text{F}_x$ has been further investigated. The magnetotransport is dominated by magnetopolarons. Magnetoresistance measurements of the series $\text{Nd}(\text{Mn}_{1-x}\text{Co}_x)\text{AsO}_{0.95}\text{F}_{0.05}$ show that doping with cobalt on the manganese site pins the magnetopolarons and suppresses the CMR, which is completely destroyed by $x = 0.047$. The chemical doping results in non-stoichiometric samples, with both As and O vacancies. The relationship between the non-stoichiometry, magnetic order, electron doping and CMR is explored. The Nd antiferromagnetic transition and simultaneous reorientation of the Mn spins into the basal plane at 23 K (T_{SR}) is not effected by Co doping. However, there is a significant decrease in $T_{\text{N}}(\text{Mn})$ as the antiferromagnetic transition is suppressed from 360 K to 300 K as x increases from 0 – 0.047. The manganese moment at 10 K is also reduced from $3.86(2) \mu_{\text{B}}$ to $3.21(2) \mu_{\text{B}}$ over the same doping range. This reduction in the in-plane Mn moment decreases the electron-electron correlations below T_{SR} and acts to further diminish the magnetoresistance.

Introduction

High temperature superconductivity has been reported in compounds containing FeAs layers, with critical temperatures (T_c) of up to 56.3 K.¹ The phenomena has been observed in several structural families of pnictides including the 1111-type $LnFeAsO$,^{2, 3} the 122 $BaFe_2As_2$ type^{4, 5} and the 111-family based on $LiFeAs$.^{6, 7} The properties of these complex magnetic systems can be heavily influenced by electron donor doping with cobalt, as partial substitution of Co for Fe in $LaFe_{1-x}Co_xAsO$ destroys the antiferromagnetic (AFM) order of the parent compound, with superconductivity emerging for samples $x \geq 0.05$ and a maximum onset temperature of 14.3 K achieved for $x = 0.11$ ⁸. Similarly, the Co-doped $NdFeAsO$ system contains a superconducting dome at doping levels 5-20% with a maximum T_c of 16.5 K.⁹ The superconducting properties of these systems appear to be sensitive to the twofold tetrahedral (α) angle of the Fe/CoAs₄ bonds. High T_c 's have generally been observed in systems where α tends towards the ideal cubic value (109.49°). Rietveld analysis describes an increase in α with cobalt doping, which may be responsible for the relatively low critical temperatures found in these electron doped systems.

In addition to superconductivity, other interesting properties have been observed in non-superconducting oxypnictide compounds such as itinerant ferromagnetism in the metal (La,Nd)CoAsO.¹⁰ Recently a new mechanism of colossal magnetoresistance (CMR) has been reported in the $NdMnAsO_{1-x}F_x$ system.¹¹ A negative magnetoresistant material exhibits a large reduction in electronic resistivity upon application of a magnetic field. Magnetoresistance, MR, is defined as $MR = ((\rho_H - \rho_0)/\rho_0)$, where ρ_0 and ρ_H are equal to the resistivity in zero and applied field respectively. Magnetoresistant materials are of technological importance and are applied in magnetoresistive sensors and spintronic devices in which electron spins are used to process information. In recent years there has been intense

study into the magnetic and electronic properties of the manganite perovskites such as $\text{La}_{1-x}\text{A}_x\text{MnO}_3$ ($\text{A} = \text{Ca}, \text{Sr}, \text{Ba}$)¹² due to the observation of colossal magnetoresistance (CMR). The manganites are remarkable as they can exhibit a change in conductivity of more than five orders of magnitude upon application of a magnetic field. The complete theory of CMR in manganese oxides is not yet established, but the largest magnetoresistance is observed in the vicinity of the paramagnetic to ferromagnetic transition, where a drop in electronic resistivity is also observed. As yet the large magnetic fields required to detect the CMR in these materials has limited its commercial implementation. An important research objective therefore is to discover new materials that exhibit CMR in low fields ($\ll 1$ T) to be employed in spintronic devices for smaller, faster, cheaper and more efficient computing applications. It is therefore vital to synthesise and investigate novel CMR materials in order to gain greater understanding of different CMR mechanisms which can then be exploited in future CMR devices.

The $\text{LnMnAsO}_{1-x}\text{F}_x$ ($\text{Ln} = \text{lanthanide}$) system is particularly important as several mechanisms for magnetoresistance have now been discovered. Variable field neutron diffraction measurements have shown that the CMR in $\text{NdMnAsO}_{1-x}\text{F}_x$ arises as a consequence of competition between an insulating antiferromagnetic phase and a paramagnetic semiconducting phase in an applied field, with a maximum CMR of -95% achieved at 3 K in a 9 T field.¹¹ Replacing Nd with Pr to produce $\text{PrMnAsO}_{1-x}\text{F}_x$ showed remarkably different results, as a sizeable negative magnetoresistance was observed below 34 K¹³ as a consequence of a structural tetragonal – orthorhombic transition driven by the Pr 4f electrons degrees of freedom. The role of the rare earth magnetism and transition metal within these systems is important as the spin reorientation of Mn ions from the c axis into the ab plane is commonly observed; inducing co-ordering of the rare earth ions.¹⁴ In $\text{NdMnAsO}_{0.95}\text{F}_{0.05}$ this spin reorientation directly influences the development of CMR below 20 K as a soft Coloumb gap is generated at the Fermi level, and Efros Shlovskii variable range

hopping is observed. Understanding the interplay of the complex magnetism within these systems is crucial in order to further tune the CMR. Here we report the synthesis, electronic and magnetic properties of several cobalt doped samples of $\text{Nd}(\text{Mn}_{1-x}\text{Co}_x)\text{AsO}_{0.95}\text{F}_{0.05}$.

Experimental

Polycrystalline samples of $\text{Nd}(\text{Mn}_{1-x}\text{Co}_x)\text{AsO}_{0.95}\text{F}_{0.05}$ with nominal doping concentrations of $x = 0.03, 0.06, 0.09$ and 0.12 were synthesised *via* a two-step solid-state reaction method. Initially, a NdAs precursor was obtained by the reaction of Nd pieces (Aldrich 99.9%) and As (Alfa Aesar 99.999%) at 900°C for 24h in an evacuated, sealed quartz tube. The resulting precursor was then reacted with stoichiometric amounts of MnO_2 , Mn, Co and MnF_2 (Aldrich 99.99%), all powders were ground in an inert atmosphere and pressed into a pellet of 10mm diameter. The pellet was placed into a Ta crucible and sintered at 1150°C for 48h, again in a quartz tube sealed under vacuum.

Room-temperature X-ray powder diffraction (XRD) patterns were collected on a PANalytical Empyrean powder diffractometer equipped with a $\text{Cu K}\alpha$ tube. Data were recorded in the range $10^\circ < 2\theta < 110^\circ$, with a step size of 0.013° .

Time-of-flight (TOF) neutron powder diffraction experiments were performed on the General Material Diffractometer (GEM) at the ISIS spallation source (Rutherford Appleton Laboratory, Harwell, Oxford, UK) on samples of ~ 2 g loaded in 8 mm vanadium cans. Data were acquired in the TOF range 500–18 000 μs using the four bank detectors with scan times of up to 2h at each temperature. Initially, data were recorded at low temperature 10 – 35 K. In order to determine $T_N(\text{Mn})$ of each sample, 15 minute variable temperature measurements were performed upon warming up to 370 K. Rietveld refinements were performed using the GSAS package.^{15, 16} Modelling of the background was performed by the shifted Chebyshev

polynomial function and the peak shapes were fitted using a Pseudo-Voigt function with back-to-back exponentials.

The dependence of the electrical resistance upon temperature and magnetic field were recorded using a Quantum Design physical property measurement system (PPMS) between 4 and 300 K in magnetic fields of 7 T.

Results and Discussion

Crystal Structure

Laboratory XRD showed that all synthesised compositions of $\text{Nd}(\text{Mn}_{1-x}\text{Co}_x)\text{AsO}_{0.95}\text{F}_{0.05}$ were of the desired 1111-pnictide phase and could be indexed on a tetragonal unit cell of space group $P4/nmm$ at 298 K. Some small weak reflections were apparent which could be assigned to MnAs and a silica-based impurity of non-magnetic $\text{Nd}_4\text{MnSi}_3\text{O}_{13}$ (presumably from reaction of the materials with vapour resulting from the quartz ampoule at high temperature). There was no evidence of any other silicate or silicon fluoride impurities.

Variable temperature neutron diffraction data were recorded for all samples in order to determine the effect of cobalt doping on the crystal and magnetic structures. Similar to $\text{NdMnAsO}_{0.95}\text{F}_{0.05}$ ¹¹ and LaMnAsO ,¹⁴ no change in crystal structure was detected down to 10 K. Rietveld refinement of the crystal and magnetic structure at 10 K for each sample were used to establish trends across the $\text{Nd}(\text{Mn}_{1-x}\text{Co}_x)\text{AsO}_{0.95}\text{F}_{0.05}$ series. Excellent fits were obtained for all x , as shown in Figure 1, with corresponding agreement factors and refined parameters presented in Table 1.

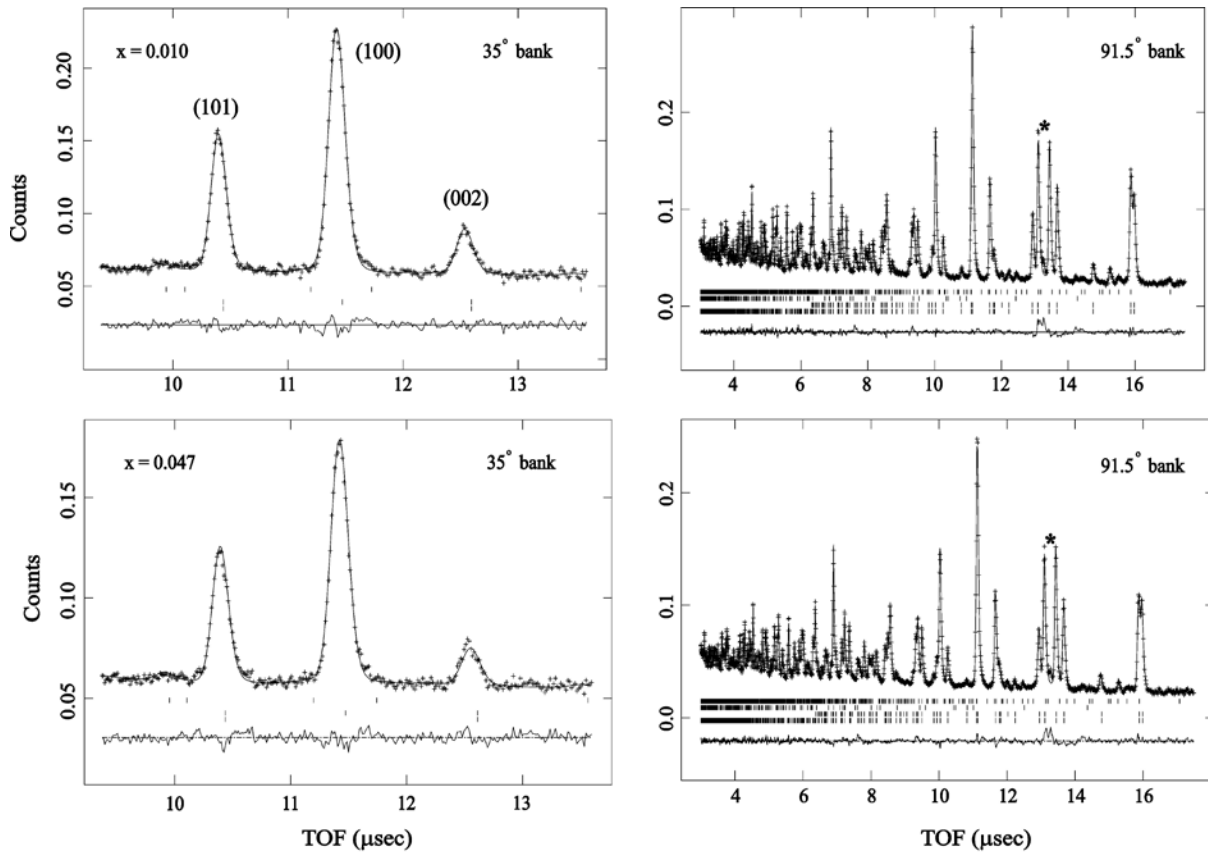


Figure 1. The Rietveld refinement fits to the $I4/mmm$ structural models of $\text{Nd}(\text{Mn}_{1-x}\text{Co}_x)\text{AsO}_{0.95}\text{F}_{0.05}$ $x = 0.010$ and 0.047 . The (101), (100) and (002) magnetic reflections observed in the 35° bank are shown alongside the overall structure obtained from the 91.5° bank. Minor secondary and tertiary phases of MnAs ($\sim 2\%$) and $\text{Nd}_4\text{MnSi}_3\text{O}_{13}$ ($\sim 3\%$) were detected and included in the fits, with a peak from the sample environment represented by the asterisk.

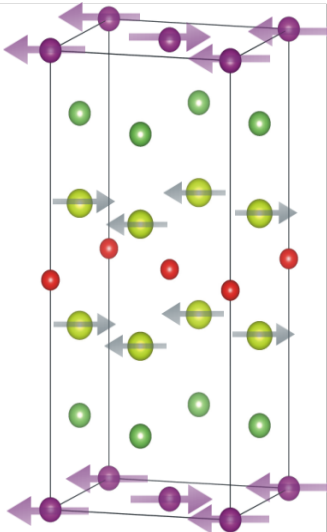
Results showed the Nd and As atoms are located at Wyckoff positions $2c$ and O/F at the $2a$ site. Co was successfully doped onto the $2b$ site, also occupied by Mn. The Co and Mn are disordered over the $2b$ site and there was no evidence of charge ordering. Refinement of the relative site occupancies showed that the nominal doping levels attempted were not achieved. The refined values indicated cobalt dopant values of $x = 0.010, 0.015, 0.034$ and 0.047 , instead of the much higher nominal values. Attempts of Co-doping BaFe_2As_2 single crystals reportedly showed cobalt precipitating out of the main matrix to form peripheral grain boundaries. Cobalt

clustering into Co-rich and Co-depleted areas was evidenced, which gave rise to large overall a lattice parameters and enhanced superconducting T_C values.¹⁷ Therefore, it is possible that cobalt has precipitated out of the samples and deposited on the surrounding silica vessel which encapsulated the pellets during the synthesis step. Varying degrees of arsenic non-stoichiometry were also observed across the $\text{Nd}(\text{Mn}_{1-x}\text{Co}_x)\text{AsO}_{0.95}\text{F}_{0.05}$ series. The undoped sample has full site occupancy, whilst cobalt doping results in As deficiencies ranging from 4.9 % - 6 %. This may be a consequence of charge-balance effects due to the aforementioned cobalt leaching from the Mn/CoAs tetrahedra. Furthermore Ta is a known As getter, therefore, the subsequent reaction of As with the Ta foil utilised in the synthesis step may have also acted to facilitate the formation of arsenic vacancies, similar to that observed in $\text{LaO}_{0.9}\text{F}_{0.1}\text{FeAs}_{1-\delta}$.¹⁸ The refined oxygen $2a$ site occupancy for each Co-doped sample was also slightly lower (~ 0.92) than the value expected (0.95). The non-stoichiometry on the As and O sites could further contribute to the electron doping of the Mn cation, although it's likely that the electrons are trapped by the vacancies. The potential average valence on the $2b$ site for each composition is given in Table 1. The Nd and F occupancies refined to within $\pm 1\%$ of the expected occupancy and were fixed in further refinement at 1 and 0.05, respectively.

The cell parameters a and c are largely invariant to doping and do not follow Vegard's Law. However, there appears to be a strong correlation between both the a and c cell parameters and the level of arsenic deficiency (Figure 2). Removing As atoms results in vacancies which form strong covalent bonds with neighbouring Mn and Co ions, clearly effecting the tetrahedra in the plane and along the c axis.¹⁹ The refined values for bond angles and interatomic distances at 10 K are shown in Table 1.

Table I: Refined cell parameters, agreement factors, atomic parameters and selected bond lengths and angles for Nd(Mn_{1-x}Co_x)AsO_{0.95}F_{0.05} from Rietveld fits against GEM high resolution neutron diffraction data at 10 K. Nd and As are at $2c$ ($\frac{1}{4}, \frac{1}{4}, z$), Mn,Co at $2b$ ($\frac{3}{4}, \frac{1}{4}, \frac{1}{2}$) and O, F at $2a$ ($\frac{3}{4}, \frac{1}{4}, 0$). Minor secondary and tertiary phases of MnAs (~2%) and Nd₄MnSi₃O₁₃ (~3%) were detected.

Atom	Occupancy		Co (x)				
			0	0.010	0.015	0.034	0.047
Nd	1.00	z	0.12994(7)	0.13096(9)	0.13163(8)	0.13208(7)	0.13116(8)
		U _{iso} (Å ²)	0.0041(5)	0.0026(2)	0.0028(2)	0.0035(2)	0.0027(2)
		μ _B (xy)	2.10(3)	1.45(2)	1.45(2)	1.38(1)	1.32(1)
Mn	y	y	1.000	0.990(3)	0.985(2)	0.966(2)	0.957(2)
		U _{iso} (Å ²)	0.0062(6)	0.0026(3)	0.0022(2)	0.0026(2)	0.0024(3)
		μ _B (xy)	3.86(2)	3.42(2)	3.49(2)	3.42(2)	3.21(2)
As	x'	x'	1.00(3)	0.935(3)	0.951(3)	0.949(3)	0.940(3)
		z	0.6742(1)	0.6734(1)	0.6739(1)	0.6742(1)	0.6734(1)
		U _{iso} (Å ²)	0.0086(5)	0.0018(2)	0.0020(2)	0.0026(2)	0.0030(2)
O/F	x''/0.05	x''	0.95(3)	0.923(3)	0.926(3)	0.921(3)	0.925(4)
		U _{iso} (Å ²)	0.0092(6)	0.0031(2)	0.0033(2)	0.0035(2)	0.0037(2)
Average Mn/Co Valence			1.950	1.700	1.755	1.739	1.720

<p style="text-align: center;">T = 10 K</p>  <p>The magnetic unit cell at 10 K, with Nd and Mn,Co magnetic spins aligned in the <i>ab</i> plane.</p>	a (Å)	4.04342(2)	4.0281(9)	4.0493(8)	4.0445(8)	4.0229(9)
	c (Å)	8.8716(2)	8.846(2)	8.892(2)	8.884(2)	8.842(2)
	χ^2 (%)	1.80	1.14	1.18	0.98	0.90
	R _{WP} (%)	4.54	3.53	3.54	3.23	3.25
	R _P (%)	4.08	2.69	2.77	2.55	2.53
	Nd-O/F (Å)	2.3273(5)	2.3233(6)	2.3387(5)	2.3381(5)	2.3217(6)
	Mn/Co-As (Å)	2.5447(6)	2.5320(8)	2.5479(7)	2.5471(7)	2.5294(8)
	Mn/Co-Mn/Co (Å)	2.8591(7)	2.8484(7)	2.8633(7)	2.8599(6)	2.8446(7)
	Nd-As (Å)	3.3456(9)	3.3328(8)	3.3448(8)	3.3374(8)	3.3284(9)
	α_1 Nd-O/F-Nd (°)	120.62(4)	120.21(4)	119.93(3)	119.75(3)	120.08(4)
	α_2 Nd-O/F-Nd (°)	104.20(2)	104.39(2)	104.51(2)	104.59(2)	104.44(2)
	α_1 As-Mn/Co-As (°)	111.64(2)	111.55(2)	111.63(2)	111.69(2)	111.57(2)
	α_2 As-Mn/Co-As (°)	105.21(4)	105.40(4)	105.25(4)	105.11(4)	105.35(4)
	Mn/CoAs Layer	3.0908(4)	3.0678(5)	3.0926(4)	3.0952(4)	3.0664(4)
Nd(O/F) Layer	2.3056(6)	2.3169(5)	2.3409(6)	2.3468(6)	2.3194(5)	

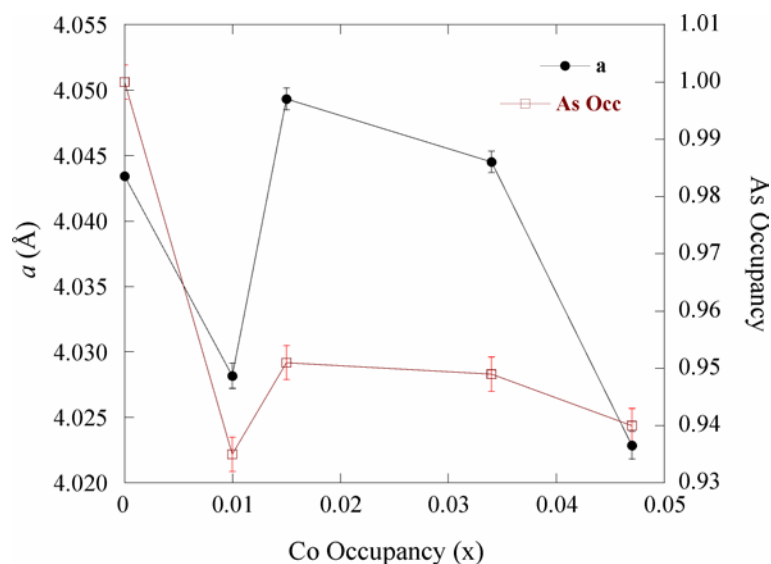


Figure 2. The variation of the lattice parameter a and arsenic site occupancy as a function of x .

The Mn-As and Mn-Mn bond lengths are largely x invariant but mirror the changes in the As content across the series. The Nd-O bond lengths behave in a similar way to the Mn-As and Mn-Mn, as the cell parameters of the unit cell are also influenced by arsenic deficiency and therefore effect the neodymium oxygen bonds in the plane and along c .

The As-(Mn,Co)-As bond angles do not vary significantly across the series. This is in contrast to cobalt doping in superconducting $Ln(Fe_{1-x}Co)_xAsO$ which tends to increase the distortion within the $FeAs_4$ tetrahedra away from the ideal environment; whereas the $MnAs_4$ tetrahedra within this system are clearly robust to structural distortions with small amounts of cobalt doping and the resulting As^{3-}/O^{2-} non-stoichiometry. The O-Nd-O bond angles mirror the evolution of the Nd z position as it changes with cobalt doping across the series (Supplementary Figure 1).

Magnetic Structure

The magnetic susceptibilities of $Nd(Mn_{1-x}Co_x)AsO_{0.95}F_{0.05}$ samples ($x = 0.010, 0.015, 0.034$ and 0.047) were measured between 5 K and 400 K on a Quantum Design SQUID magnetometer

in an applied field of 100 Oe after zero-field cooling (ZFC). Due to traces of the ferromagnetic impurity, MnAs, the data were dominated by a broad ferromagnetic transition at ~ 320 K. Attempts to fully extract the susceptibility of the MnAs impurity were unsuccessful due to the problems encountered in our previous study of $\text{Nd}_{1-x}\text{Sr}_x\text{MnAsO}$.²¹

Acquisition of variable temperature high resolution neutron diffraction data allowed for the determination of the Néel temperatures and magnetic structure of each doped material. The (101) and (100) magnetic reflections emerge at temperatures $\leq T_N(\text{Mn})$. Upon cooling the (101) reflection is reduced compared to the (100) and an increase in intensity of the (002) peak is observed as the Nd^{3+} spins order antiferromagnetically and the Mn spins reorient into the basal plane (Figure 1). There is no change in magnetic structure as x increases; with the AFM ordering of manganese along c at temperatures ≥ 300 K (Figure 3), along with the Nd ordering and spin reorientation transition (T_{SR}) of the Mn spins into the basal plane at 23 K (Table 1). T_{SR} is not effected by Co doping, however, there is a significant decrease in $T_N(\text{Mn})$ with increasing cobalt content as the transition is suppressed from 360 K to 300 K as x increases from 0 – 0.047 (Figure 3).

It has previously been reported that electron doping by substitution of H^- for O^{2-} in $\text{LaMnAsO}_{1-x}\text{H}_x$ destroys the antiferromagnetic order of the Mn spins. Ferromagnetic order is observed for $x \geq 0.08$ with a simultaneous transition from the semiconducting to the metallic phase.²⁰ Hole doping $\text{Nd}_{1-x}\text{Sr}_x\text{MnAsO}$ results in a reduction in $T_N(\text{Mn})$ from 360 K for $x = 0$ to 325 K for $x = 0.1$.²¹ In contrast, the application of external pressure on $\text{NdMnAsO}_{0.95}\text{F}_{0.05}$ acts to enhance $T_N(\text{Mn})$ from 360 K to 383 K due to a reduction of the Mn-As bond length and interlayer spacing, which consequently enhances superexchange between Mn centres.²² As there appears to be no strong correlation between the structural parameters and cobalt content in $\text{Nd}(\text{Mn}_{1-x}\text{Co}_x)\text{AsO}_{0.95}\text{F}_{0.05}$, the sharp reduction in $T_N(\text{Mn})$ is most likely a consequence of the increase in magnetic frustration and electron doping upon substitution of Co into the $(\text{MnAs})^-$ layer.

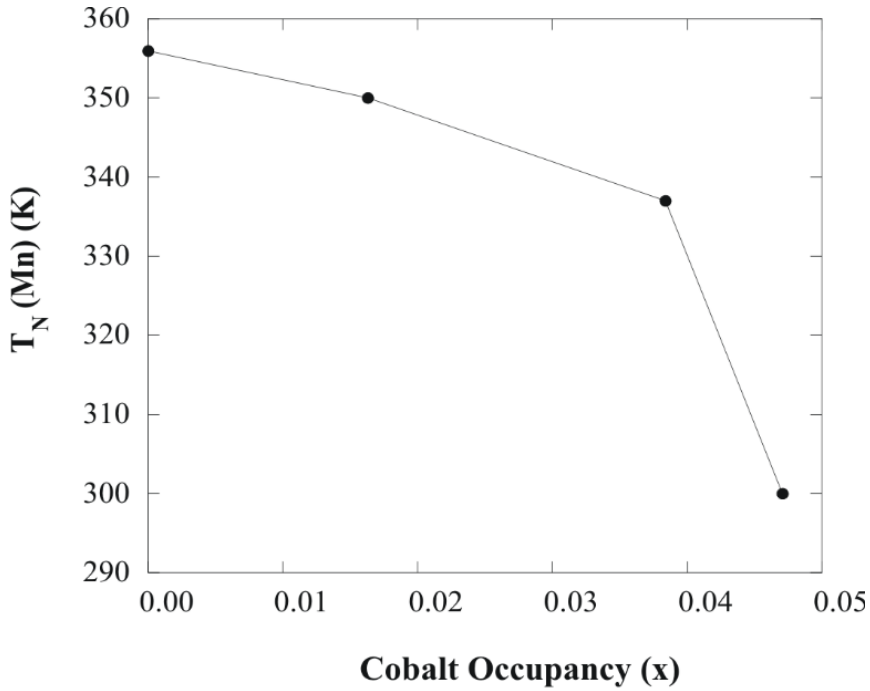


Figure 3. The variation of $T_N(\text{Mn})$ with increasing cobalt content in $\text{NdMn}_{1-x}\text{Co}_x\text{AsO}_{0.95}\text{F}_{0.05}$.

Figure 4 presents the variation of the Mn moment at 10 K with x . The moment on the $2b$ site is reduced from $3.86(2) \mu_B$ to $3.21(2) \mu_B$ as x increases from 0 to 0.047. There is a clear correlation between the magnitude of the ordered Mn moment and the arsenic occupancy across the series (Figure 4). The same relationship is not evident between the level of Co doping and/or the oxygen deficiency and the magnitude of the ordered Mn moment across the series. The removal of As atoms from the MnAs_4 tetrahedra results in a reduction of available nearest-neighbour antiferromagnetic superexchange pathways, and also increases the electron doping of the Mn site. These combined processes, coupled with the Co substitution, act to enhance magnetic frustration and reduce the ordered moment. This is similar to 3d magnetic oxides where oxygen deficiency results in a reduction of the transition metal moment.^{23, 24} The inset of Figure 4 shows the variation of the Nd moment with x at 10 K. The Nd antiferromagnetic order is induced by the Mn antiferromagnetism at T_{SR} ²⁵ and is therefore strongly magnetically

coupled with the Mn moment, so that the Nd moment reduces from 2.10 – 1.32 μ_B over the same doping range.

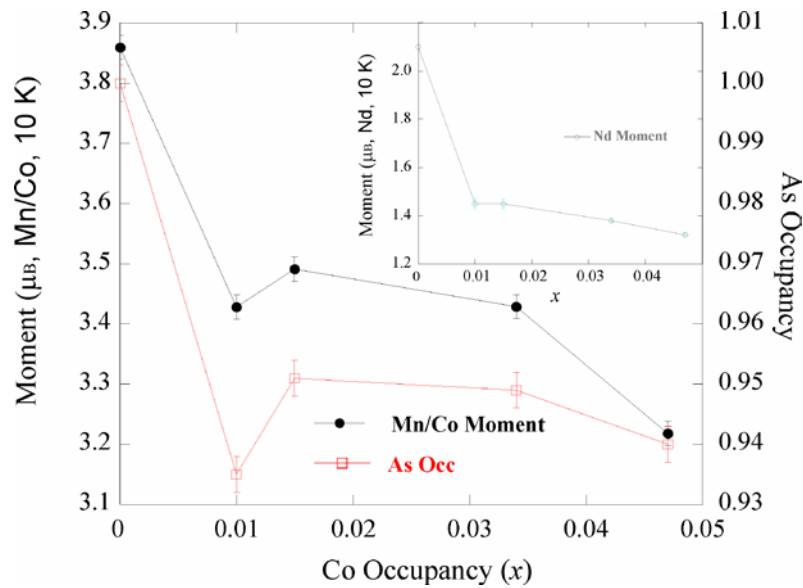


Figure 4. The variation of the Mn/Co magnetic moment at 10 K with x . The variation of the arsenic occupancy with x is also shown, highlighting the correlation between the two parameters across the series. The inset shows the variation of the Nd magnetic moment with x .

Electronic Properties

A maximum CMR of -95% was reported for the $\text{NdMnAsO}_{1-x}\text{F}_x$ system at $x = 0.05$ in a 9 T field.¹¹ In order to establish how the substitution of Co for Mn tunes the CMR, variable temperature and field resistivity measurements were performed on all samples of $\text{Nd}(\text{Mn}_{1-x}\text{Co}_x)\text{AsO}_{0.95}\text{F}_{0.05}$. All samples are semi-conducting at 290 K with measured resistivities between 1 and 40 $\Omega\cdot\text{cm}$. The variation of MR with cobalt content can be seen in Figure 5. The MR is rapidly diminished as the Co doping increases from $x = 0 - 0.047$. There is no clear relationship between the variation of the -MR with x and the changes in crystal and magnetic structure reported above.

There appear to be at least two mechanisms of MR present in the $\text{Nd}(\text{Mn}_{1-x}\text{Co}_x)\text{AsO}_{0.95}\text{F}_{0.05}$ oxypnictides ($x = 0 - 0.015$). Below ~ 80 K the $-\text{MR}$ increases exponentially. The variation of $-\text{MR}$ with temperature for the $\text{Nd}(\text{Mn}_{1-x}\text{Co}_x)\text{AsO}_{0.95}\text{F}_{0.05}$ phases ($x = 0 - 0.015$) below 80 K suggests that the magnetotransport is dominated by magnetic polarons. A characteristic of negative magnetoresistance mediated by magnetic polarons is an exponential rise in $-\text{MR}$ with decreasing temperature²⁶ since the $-\text{MR}$ arises from an activated transport process. The large negative magnetoresistance observed in $\text{RuSr}_2\text{Nd}_{1.8-x}\text{Ce}_x\text{Y}_{0.2}\text{Cu}_2\text{O}_{10-d}$ ^{27, 28, 29} and EuB_6 ³⁰ can be explained by a magnetopolaron model. When the local exchange coupling is large enough and the density of carriers is low, charge carriers can be localised by magnetic clusters to form magnetopolarons. When a magnetic field is applied the size of the magnetic polarons increases so that the polarons overlap which leads to a reduction in charge localisation and hence large negative magnetoresistance.

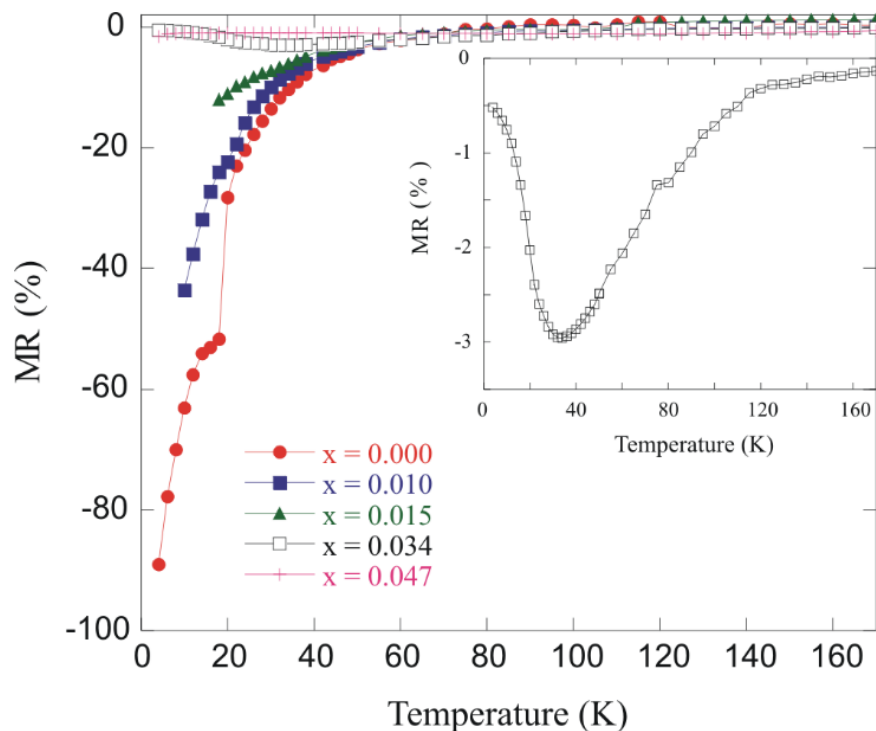


Figure 5. The variation of the 7 T magnetoresistance (MR) with temperature for $\text{Nd}(\text{Mn}_{1-x}\text{Co}_x)\text{AsO}_{0.95}\text{F}_{0.05}$. The inset shows the low temperature MR observed for $x = 0.034$.

The magnetotransport measurements on the $\text{Nd}(\text{Mn}_{1-x}\text{Co}_x)\text{AsO}_{0.95}\text{F}_{0.05}$ phases show that as the temperature is reduced below 75 K, $-\text{MR}_{7\text{T}}$ rises exponentially. This suggests that magnetopolarons are forming within the antiferromagnetic matrix. The formation of a magnetopolaron arises as the energy of a charge carrier is minimal for ferromagnetic ordering. The carrier therefore produces a ferromagnetic microregion within the antiferromagnet matrix and becomes self-trapped.³¹ Upon application of a magnetic field the Mn spins cant into the direction of the magnetic field¹¹ so that the magnetic polarons become delocalised and the resistivity decreases in field.

For $x = 0.000, 0.010$ and 0.015 , above 75 K the electron transport is dominated by thermally activated charge carriers across a band gap (E_g), according to the relationship $\rho = \rho_0 \exp(E_g/2kT)$, where ρ is the measured resistivity, k the Boltzmann constant and T is the temperature with corresponding activation energies of $E_g = 23$ meV, 45 meV and 64 meV (Figures S3 and S5). It has recently been shown that if a system has sizeable disorder of magnetic energies, then the transport can be modelled as magnetopolaron hopping which can be described as a stretched exponential³² similar to Mott variable range hopping. In the absence of Coulomb correlations, the transport can be modelled by $\ln(\rho/\rho_0) = (\tilde{T}/T)^p$ where $p = 2/(d+2)$ and d is the dimensionality of the system. For a three dimensional (3D) system therefore $p = 0.4$.³² For $x = 0 - 0.015$, between 75 K and the spin reorientation transition at ~ 23 K the data could be well modelled by 3D spin-polaron hopping of the charge carriers (Figures S2, S4 and S6). A much better fit was obtained to the 3D magnetopolaron hopping model than to the Mott three-dimensional variable range hopping (3D VRH) equation ($\rho = \rho_0 \exp(T_0/T)^{0.25}$) with $\tilde{T} = 4.07 \times 10^3$ K, 1.44×10^4 K and 2.98×10^4 K for $x = 0.000, 0.010$ and 0.015 respectively. $\tilde{T}^{(d)} = \left[\frac{\beta_0^{(d)}}{Ga^d} \right]$, where β_0 is a numerical factor of the order of unity, G is the joint density of polaronic states and a is the localisation radius of the electron wave function.³² The increase in \tilde{T} with

increasing x corresponds to a decrease in the localisation radius and would suggest that Co doping pins the magnetopolarons restricting their transport. This is most likely a consequence of the electronic disorder brought about by Co substitution onto the MnAs plane and the resulting As vacancies.

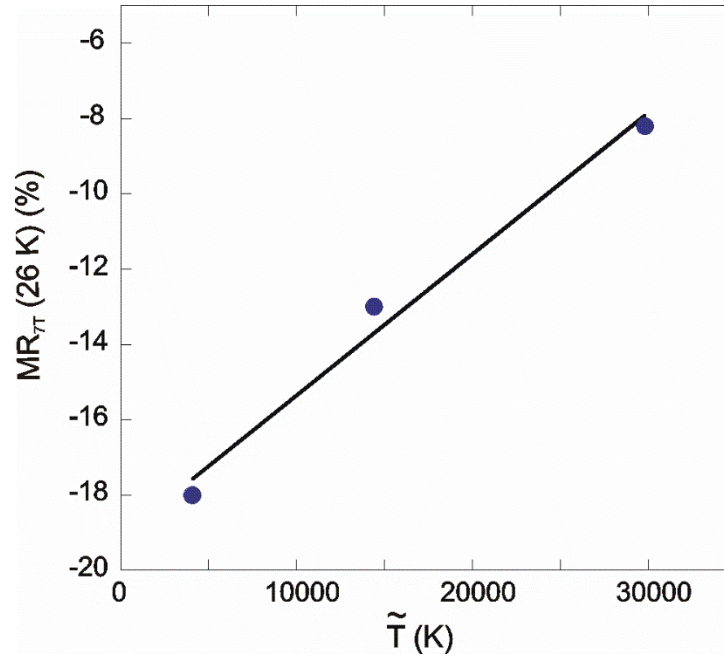


Figure 6 Variation of the 7T magnetoresistance at 26 K with \tilde{T} showing that as x increases from 0 – 0.015. \tilde{T} increases with a concomitant reduction in the magnitude of the $-MR$.

Figure 6 shows the variation of $-MR$ with \tilde{T} where a linear relationship between the $-MR$ and \tilde{T} is observed so that above T_{SR} the magnitude of the $-MR$ decreases with increasing \tilde{T} . This would suggest that the pinning of the magnetopolarons by the Co impurities restricts the growth of the magnetopolarons upon applying a magnetic field, suppressing the $-MR$.

For $NdMnAsO_{0.95}F_{0.05}$, between 23 K (T_{SR}) and 4 K the resistivity data can be fit to the Efros-Shklovskii (ES) VRH equation ($\rho/\rho_0 = \exp[T_{ES}/T]^{1/2}$), with $T_{ES} = 922$ K¹¹. For $x \geq 0.01$ Efros-Shklovskii behaviour is no longer observed and the data below T_{SR} can still be modelled by the 3D magnetopolaron hopping equation, although a change in gradient is apparent at T_{SR} so that

\tilde{T} increases to 2.09×10^4 (Figure S7). This would suggest that the reorientation of the Mn spins into the *ab* plane further decreases the localisation radius of the magnetopolaron. For $x = 0.015$ the sample is too resistive to measure below 18 K but an excellent fit to the magnetopolaron hopping model is observed down to 18 K (Figure S6).

For $\text{NdMnAsO}_{0.95}\text{F}_{0.05}$, the $-\text{MR}$ rises sharply below T_{SR} as previously reported.¹¹ Below T_{SR} , the reorientation of the Mn moment into the *ab* plane results in enhanced electron-electron correlations so that ES variable range hopping is observed. Application of a 7 T magnetic field results in a reduction of the in-plane Mn moment from $3.83(2) \mu_{\text{B}}$ to $3.56(2) \mu_{\text{B}}$,¹¹ suppresses the electron-electron correlations and hence further enhances the $-\text{MR}$. This sharp increase in the magnitude of the $-\text{MR}$ is not apparent for $x > 0$ (Fig. 5), although an inflection in the $-\text{MR}$ is observed at T_{SR} for $x = 0.010$ and 0.015 (Figure 5). ES VRH is no longer observed for $x \geq 0.01$ so that there is a reduction in electron-electron correlations upon Co doping. Upon substitution of 1% Co for Mn, the in-plane Mn moment at 10 K reduces from $3.86(2) \mu_{\text{B}}$ to $3.42(2) \mu_{\text{B}}$ (Table 1, Figure 4). This 11% reduction in the ordered in-plane Mn magnetic moment with Co doping decreases the electron-electron correlations with the consequence that the $-\text{MR}$ is no longer enhanced below T_{SR} in $\text{NdMn}_{1-x}\text{Co}_x\text{AsO}_{0.95}\text{F}_{0.05}$ ($x \geq 0.01$).

There's no evidence of magnetopolaron transport for $x > 0.015$ as the electron doping increases. MR from magnetopolarons is predicted to only observed be over a very narrow doping range.²⁶ The inset of Figure 3 shows an expansion of MR data for $x = 0.034$, where a small peak of -3% MR can be seen at 34 K. There is no evidence of MR for $x = 0.047$. The $\rho(T)$ data for both of these compositions contain broad transitions at 16 K and 130 K for $x = 0.034$ and 0.047 respectively, shown in the inset of Figure S8. Below these temperatures there is a change in the electronic behaviour, with a decrease in resistivity observed upon further cooling indicating a metallic temperature dependence; characteristic of a degenerate

semiconductor. This generally occurs when a semiconducting system has become sufficiently doped with charge carriers that it behaves more like a metal than a semiconductor as the Fermi-level moves within the vicinity of the conduction band, and is likely a consequence of the substantial electron doping induced by Co, As and O vacancies. This has been reported for other layered Mn pnictides such as BaMn_2As_2 .³³ There is no evidence of ferromagnetic order as reported for electron doped $\text{LaMnAsO}_{1-x}\text{H}_x$ ²⁰, where ferromagnetic metallic behaviour is observed for $x > 0.08$. The $\text{NdMn}_{1-x}\text{Co}_x\text{AsO}_{0.95}\text{F}_{0.05}$ phases remain semiconducting for all x which would suggest that the majority of electrons generated by the As^{3-} and O^{2-} non-stoichiometry are trapped by the anionic vacancies.

Conclusions

The results demonstrate that the CMR of the $\text{NdMnAsO}_{0.95}\text{F}_{0.05}$ parent compound is suppressed by the substitution of Co for Mn in $\text{Nd}(\text{Mn}_{1-x}\text{Co}_x)\text{AsO}_{0.95}\text{F}_{0.05}$. Small amounts of Co-doping rapidly diminish the MR for samples $x = 0.010$ and 0.015 , and the phenomenon is no longer observed for $x = 0.047$. The results confirm that the magnetotransport is dominated by magnetopolarons and that large magnetoresistances are only observed over a very narrow doping range ($x = 0 - 0.015$). Degenerate semiconducting behaviour is observed for samples $x \geq 0.034$. The magnetic exchange interactions become increasingly frustrated with increasing Co doping and the simultaneous As non-stoichiometry, across the series. The reduced exchange pathways and electron doping lead to the significant reduction of the in-plane Mn/Co magnetic moment. The study reveals that, while the crystal lattice is fairly robust to cobalt doping; the CMR properties are highly sensitive to small perturbations of the Mn magnetic moment.

Electronic supplementary information (ESI) available: The ESI includes figures showing the variation of the Nd-O-Nd angle variance with x , fits to the resistivity data (Arrhenius,

magnetopolaron and variable range hopping models) and variable temperature resistivity data for all x .

Corresponding Author

*a.c.mclaughlin@abdn.ac.uk

Tel: 0044 1224272924; Fax: 0044 1224272921

Conflicts of Interest

There are no conflicts of interest.

Acknowledgements

This research is supported by the EPSRC (research grant EP/L002493/1). We also acknowledge the UK Science and Technology Facilities Council (STFC) for provision of beam time at ISIS.

References

-
- ¹ C. Wang, L. Li, S. Chi, Z. Zhu, Z. Ren, Y. Li, Y. Wang, X. Lin, Y. Luo, S. Jiang, X. Xu, G. Cao and Z. Xu, *Z. Europhys. Lett.*, 2008, **83**, 67006.
 - ² G. F. Chen, Z. Li, D. Wu, J. Dong, G. Li, W. Z. Hu, P. Zheng, J. L. Luo and N. L. Wang, *Chin. Phys. Lett.*, 2008, **25**, 2235-2238.
 - ³ Z. A. Ren, J. Yang, J. W. Lu, W. Yi, G. C. Che, X. L. Dong, L. L. Sun and Z. X. Zhao, *Mater. Res. Innov.*, 2008, **12**, 105-106.
 - ⁴ P. L. Alireza, Y. T. C. Ko, J. Gillett, C. M. Petrone, J. M. Cole, G. G. Lonzarich, and S. E. Sebastian, *J. Phys. Condens. Matter.*, 2008, **21**, 012208.
 - ⁵ A. Mani, N. Ghosh, S. Paulraj, A. Bharathi and C. S. Sundar, *Europhys. Lett.*, 2009, **87**, 17004.

-
- ⁶ M. J. Pitcher, D. R. Parker, P. Adamson, S. J. C. Herkelrath, A. T. Boothroyd and S. J. Clarke, *Chem. Commun.*, 2008, 5918 – 5920.
- ⁷ X. C. Wang, Q. Q. Liu, Y. X. Lv, W. B. Gao, L. X. Yang, R. –C. Yu, F. Y. Li and C. Q. Jin, *Solid. State. Commun.*, 2008, **148**, 538 – 540.
- ⁸ A. S. Sefat, A. Huq, M. A. McGuire, R. Jin, B. C. Sales, D. Mandrus, L. M. D. Cranswick, P. D. Stephens and K. H. Stone, *Phys. Rev. B*, 2008, **78**, 104505.
- ⁹ A. Marcinkova, D. A. M. Grist, I. Margiolaki, T. C. Hansen, S. Margadonna and J. –W. G. Bos, *Phys. Rev. B*, 2010, **81**, 064511.
- ¹⁰ A. Pal, M. Tropeano, M. Hussain, H. Kishan and V. P. S. Awana, *J. Appl. Phys.*, 2011, **109**, 07E121.
- ¹¹ E. J. Wildman, J. M. S. Skakle, N. Emery and A. C. McLaughlin, *J. Amer. Chem. Soc.*, 2012, **134**, 8766-8769.
- ¹² C. N. R. Rao and B. Raveau, (Eds.) Colossal Magnetoresistance, Charge Ordering and Related Properties of Manganese Oxides, (World Scientific, Singapore, 1998).
- ¹³ E. J. Wildman, F. Sher and A. C. McLaughlin, *Inorg. Chem.*, 2015, **54**, 2536-2542.
- ¹⁴ N. Emery, E. J. Wildman, J. M. S. Skakle, A. C. McLaughlin, R. I. Smith and A. N. Fitch, *Phys. Rev. B*, 2011, **83**, 144429.
- ¹⁵ H. M. Rietveld, *Acta Crystallogr.*, 1967, **22**, 151-152.
- ¹⁶ A. C. Larson and R. B. V. Dreele, General structure analysis system (GSAS), Los Alamos National Laboratory Report, 1994, 86-748.
- ¹⁷ L. Li, Q. Zheng, Q. Zou, S. Rajput, A. O. Ijaluola, Z. Wu, X. P. Wang, H. B. Cao, S. Somnath, S. Jesse, M. Chi, Z. Gai, D. Parker and A. S. Sefat, *Sci. Rep.*, 2017, **7**, 949.
- ¹⁸ G. Fuchs, S. L. Drechsler, N. Kozlova, G. Behr, A. Kohler, J. Werner, K. Nenkov, R. Klingeler, J Hamann-Borrero, C. Hess, A. Kondrat, M. Grobosch, A. Narduzzo, M. Knupfer, J. Freudenberger, B. Buchner and L. Schultz. *L. Phys. Rev. Lett.*, 2008, **101**, 237003.

-
- ¹⁹ K. Kikoin and S. J. Drechsler, *J. Magn. Magn. Mater.*, 2012, **324**, 3471-3475.
- ²⁰ T. Hanna, S. Matsuishi, K. Kodama, T. Otomo, S. –I. Shamoto and H. Hosono, *Phys. Rev. B*, 2013, **87**, 020401.
- ²¹ E. J. Wildman, N. Emery and A. C. Mclaughlin, *Phys. Rev. B*, 2014, **90**, 224413.
- ²² E. J. Wildman, M. G. Tucker and A. C. Mclaughlin, *J. Phys. Condens. Matter.*, 2015, **27**, 116001.
- ²³ S.V. Trukhanov, A.V. Trukhanov, A.N. Vasiliev and H. Szymczak, *JETP*, 2010, **111**, 209.
- ²⁴ S.V. Trukhanov, A.V. Trukhanov, A.N. Vasiliev, A.M. Balagurov, H. Szymczak, *JETP*, 2011, **113**, 819.
- ²⁵ C. Lee, E. Kan, H. Xiang, R. K. Kremer, S. –H. Lee, Z. Hiroi and M. –H. Whangbo, *Inorg. Chem.*, 2012, **51**, 6890-6897.
- ²⁶ P. Majumdar and P. Littlewood, *Phys. Rev. Lett.*, 1998, **81**, 1314.
- ²⁷ A. C. Mclaughlin, F. Sher and J. P. Attfield, *Nature* (London), 2005, **436**, 829; A. C. Mclaughlin, F. Sher and J. P. Attfield, *Nature* (London), 2005, **437**, 1057
- ²⁸ A. C. Mclaughlin, L. Begg, C. Harrow, S. A. J. Kimber, F. Sher and J. P. Attfield, *J. Am. Chem. Soc.*, 2006, **128**.
- ²⁹ A. C. Mclaughlin, F. Sher, S. Kimber and J. P. Attfield, *Phys. Rev. B*, 2007, **76**, 094514.
- ³⁰ M. J. Calderón, L. G. L. Wegener and P. B. Littlewood, *Phys. Rev. B*, 2004, **70**, 092408.
- ³¹ E. L. Nagaev, *Zh. E. Ksp. Teor. Fiz.*, 1967. **6**, 484
- ³² M. Foygel, R. D. Morris and A. G. Petukhov, *Phys. Rev. B*, 2003, **67**, 134205.
- ³³ Y. Singh, A. Ellern and D. C. Johnston, *Phys. Rev. B*, 2009, **79**, 094519.